PCCP

Accepted Manuscript

ROYAL SOCIETY OF CHEMISTRY

www.rsc.org/pccp

Journal Name

ARTICLE

Preparation of uniform Si nanoparticles for high-performance Li-ion battery anodes

Received 00th January 20xx,
Accepted 00th January 20xx

DOI: 10.1039/x0xx00000x

www.rsc.org/

Lin Sun, Tingting Su, Lei Xu, and Hong-Bin Du*

Nanostructured silicon has attracted a great deal of attention as an excellent anode material for Li ion batteries (LIBs). However, the use of Si nanomaterials in LIBs is severely hindered by their preparative methods owing to the high cost, low yield, and harsh synthetic conditions. Herein, we report a new method for the synthesis of uniform Si nanocrystals based on the magnesiothermic reduction of natural attapulgite clay. The obtained Si nanocrystals with uniform sizes of ca. 10 nm are coated with polypyrrole (denoted as ppy@Si) and show excellent electrochemical performance as anode materials for LIBs. After charging-discharging for 200 cycles at a current density of 0.6 A g^{-1}, the specific capacity value of the ppy@Si anode is ~954 mAh g^{-1}. Because of the abundance of the attapulgite, the obtained silicon nanoparticles can be exploited as a practical anode material for high-performance Li-ion battery.

1. Introduction

Lithium ion batteries (LIBs) with high energy density, no memory effect, long life and low cost have been rapidly developed for a wide range of applications such as portable electronics, electric vehicles, implantable medical and wearable devices.[1-4] Compared to traditional anodes such as graphite, silicon (Si) has attracted a great deal of attention as an excellent anode material for LIBs due to its high theoretical gravimetric capacity of ~4200 mAh g^{-1} and relatively low discharge potential.[5-7] However, the cyclic performance of Si anode is very poor because Si exhibits volume changes of ~300% upon lithium alloying and de-alloying, which will result in fracture and loss of electrical contact, and an unstable solid electrolyte interphase (SEI) growth on the Si surface.[8-10] To tackle the problem, Si nanoparticles (NPs) have been employed as anode materials for LIBs because nano-scaled structures not only effectively address the pulverization issue of Si anode, but also allow high operation rate.[11-13]

Although the abundance of Si element in nature is worth exciting, the applications of Si nanoparticles are restricted to their preparation methods. The traditional approaches to obtain Si nanoparticles and nanowires, such as chemical vapor deposition (CVD) and noble metal-assisted growth, are usually associated with high cost and low yield.[14,15] Si nanoparticles and nanowires can also be synthesized in organic solvents, but the harsh water- and oxygen-free synthetic conditions hinder their practical applications.[16-18] Recently, SiO_2 has been used as hard templates to form Si anode materials via magnesiothermic reaction, which features feasible operations and scalable applications.[19,20] However, the preparation of a low-cost SiO_2 precursor with uniform and nanometer sizes for Si nanoparticles remains a challenge.

Up to now, several methods for preparing Si micro- and nano materials from natural resources have been reported. For example, Favors *et al*. and Kim *et al*. have reported on the synthesis of Si with multi-pores and sheet-like structures from sand, respectively.[21,22] Jung *et al*. and Xing *et al*. prepared porous Si nanomaterials from rice husk and investigated their electrochemical properties as LIB anodes;[23,24] More recently, Liu *et al*. employed a magnesiothermic reduction method for facile production of three-dimensional porous Si with excellent electrochemical performance from natural reed leaves.[25] Although the above mentioned SiO_2 precursors from natural resources can produce Si micro- or nanomaterials, unfortunately, the obtained Si materials usually exhibit various sizes or irregular shapes because of the heterogeneity of such afforded SiO_2 precursors.

Herein, we report the direct synthesis of gram-grade Si sphere-like nanocrystals with uniform size around 10 nm via a magnesiothermic reduction of natural attapulgite. Because of the uniform fiber-like morphology of attapulgite, the obtained yellow Si nanoparticles show a relatively uniform size distribution. Moreover, after polypyrrole (ppy) coating, the nanocomposites (denoted as ppy@Si) exhibit excellent electrochemical performance as anode materials for LIBs, with the specific discharge capacity maintained at ~954 mAh g^{-1} after 200 cycles at constant current densities of 0.6 A g^{-1}.

2. Experimental Section

[a] State Key Laboratory of Coordination Chemistry, Collaborative Innovation Center of Chemistry for Life Sciences, School of Chemistry and Chemical Engineering, Nanjing University, Nanjing, 210023, China. E-mail: hbdu@nju.edu.cn.

† Electronic Supplementary Information (ESI) available: additional SEM, TEM, TG and charge-discharge curves.
See DOI: 10.1039/x0xx00000x

2.1 Synthetic procedures

2.1.1 Materials

Attapuligite clay was provided by Xuyi Botu Attapuligite Clay Hi-tech Development Co., Ltd., China. Metallic Mg powders with 99 % purity were purchased from Sigma Aldrich. Battery-grade ethylene carbonate (EC), diethyl carbonate (DEC), vinylene carbonate (VC) and $LiPF_6$ were purchased from Shenzheng Kejingstar Technology Ltd., China, and used as received without further purification.

2.1.2 Extraction of SiO_2 from Attapuligite clays

10 g of as-received attapuligite were passed through a 200-mesh sieve and then heated in a muffle furnace at 700 °C for 5 h. The obtained powder was added to 300 mL of HCl solution (2 M) and the reaction was maintained at 60 °C for 30 h. The obtained sample was filtered, washed with large amount of distilled water, and dried at 80 °C overnight to produce 6.7 g of SiO_2.

2.1.3 Preparation of Si NPs from SiO_2

A magnesiothermic reaction was employed to obtain Si NPs from SiO_2 nanorods. Typically, 1.4 g of Mg powders were spread uniformly on the bottom of a ceramic crucible and equivalent mass of the obtained SiO_2 nanofibers were loaded on a porous stainless steel net. The distance between the net and the bottom of crucible was less than 1 cm. The ceramic crucible was heated at 10 °C /min in a tube furnace to 500 °C for 10 min and then at 5 °C /min to 800 °C for 3 h in a flowing Ar (90 Vol %)/H_2 (10 Vol %) mixture gas. After cooling to room temperature naturally, the obtained brownish black powder was stirred in 1 M HCl–EtOH for 7 h and 6% HF solution for 15 min, respectively. The product was filtered, washed with distilled water and ethanol and dried at 60 °C in vaccum to yield 0.6 g of Si NPs.

2.1.4 Synthesis of the ppy@Si nanocomposites

0.2 g of the prepared Si NPs were dispersed in 130 mL of distilled water containing sodium dodecylsulfate (SDS, 12.5 mg) by ultrasonication for at least 20 min, followed by stirring for 12 h. Then, 875 μL of pyrrole monomer and 1.25 mL of 1 M HCl were successively added into the obtained Si NP suspension. Afterward, 0.285 g of $(NH_4)_2S_2O_8$ (dissolved in 5 mL H_2O) was added dropwise into the dispersion to induce the polymerization process. After the mixture was stirred in an ice/water bath for 3 h, the formed black powders (denoted as ppy@Si) were filtered and washed with water for several times. The final product was dried in vaccum at 60°C overnight.

2.2 Electrochemical measurements

CR2025 cells were assembled in an argon-filled glove box to perform the electrochemical experiments. The electrode was composed of 80 wt% of active material, 10 wt% of conductive graphite, and 10 wt% of sodium carboxymethyl cellulose (CMC) as a binder. The mixture was stirred in water and blade-coated on a piece of Cu foil. After drying at 85 °C in vaccum for 12 h, the foil was cut into disks of 12 mm in diameter. The mass loading of the active material was about 0.8 mg cm^{-2}. The electrolyte consisted of a solution of 1 M $LiPF_6$ in a mixture of 1:1 (v/v) EC/DEC with 2 wt % VC. Pure Li foils were served as counter electrodes and polypropylene macroporous films (Celgard 2400) as separators. The discharge-charge measurements were performed on a Neware battery testing device (Shenzheng, China) at a constant current mode over the range of 0.01−1.5 V. Cyclic voltammetry (CV) of the as-prepared anodes were measured on a CHI650d (Shanghai Chenhua CH Instruments, Inc., China) electrochemical station by using a three-electrode cell with a scanning rate of 0.2 mV s^{-1}. The specific gravimetric capacity was calculated based on per gram of ppy@Si nanocomposite.

2.3 Characterization

Powder X-ray diffraction (PXRD) measurements were taken on a Bruker D8 Advance instrument with a Cu Kα radiation (λ = 1.5418 Å). Scanning Electron Microscope (SEM) images and Energy Dispersive Spectroscopy (EDS) were obtained on a Hitachi S–4800 field-emission scanning electron microscope. Transmission Electron Microscopy (TEM) analysis was carried out with JEM-200CX equipment. Thermogravimetric (TG) analyses were performed on a simultaneous STA449F3 thermal analyzer under flowing oxygen. Fourier-transformed infrared (FT-IR) spectra were measured on a FT-IR spectrometer (Vector22) with the KBr pellet method. Raman spectroscopy (LabRAM Aramis, Horiba) equipped with 632.8 nm laser was used to investigate the structure of silicon nanoparticles. Nitrogen sorption isotherms were collected at 77 K (Micrometrics ASAP 2020 analyzer) after vaccum degassing of the sample at 200 °C for 8 h.

Results and discussion

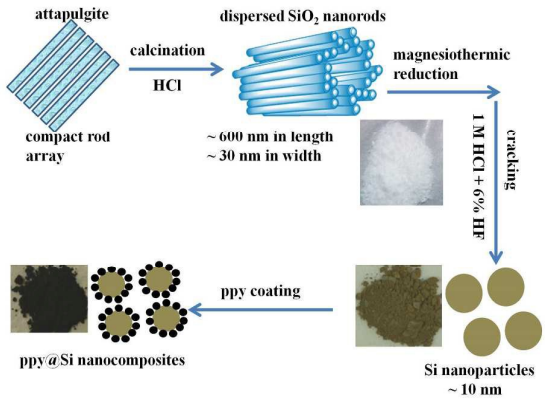

Fig. 1 Schematic illustration of the preparation of the ppy@Si nanocomposites.

Fig. 1 shows the schematic illustration of the general preparation process of ppy@Si nanocomposites from natural attapulgite. The mineral attapulgite with an ideal composition of $Si_8O_{20}Mg_5(OH)_2(H_2O)_4{\cdot}4H_2O$ is a hydrated magnesium phyllosilicate with fibrous morphology. It consists of a double chain of Si–O tetrahedra, which is linked along the edges by a layer of octahedral magnesium atoms to form a network of strips.[26] Magnesium in the mineral is often partially replaced by aluminum, iron, and/or other elements, giving rise to a variable

composition of attapulgite. The as-received mineral is mainly comprised of bundles of nanorods of attapulgite (**Fig. S1** in ESI), contaminated by some impurities, such as quartz and calcium magnesium carbonates (**Fig. 2a**). After treated with dilute acid and calcinated at 700°C in air for 2 h to remove some impurities, the structure of attapulgite was converted into an amorphous phase. The formed white powders were identified as amorphous SiO_2, together with little amount of quartz (**Fig. 2b**), while the shape remained as nanorods (**Fig. 3a**). The nanorods were well dispersed, with the length of ~600 nm and the width of ~30 nm. The pre-treated samples of attapulgite were then subject to magnesiothermic reduction according to the reaction:

$$2Mg\ (g) + SiO_2\ (s) \longrightarrow 2MgO\ (s) + Si\ (s) \qquad (1)$$

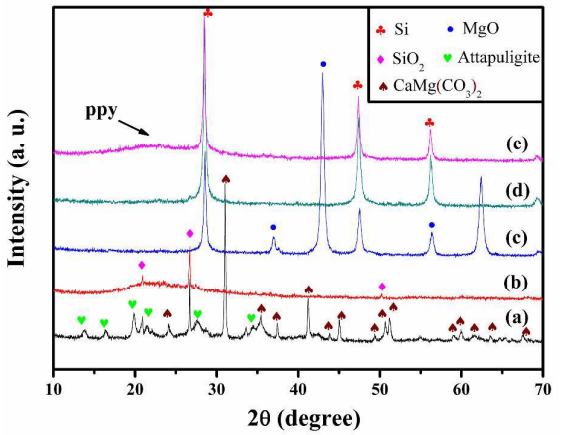

Fig. 2 XRD patterns of (a) the pristine attapulgite; (b) the obtained SiO_2 precursor; (c) the product after magnesiothermic reduction; (d) Si nanoparticles after HCl and dilute HF treatment, and (e) the ppy@Si nanocomposites.

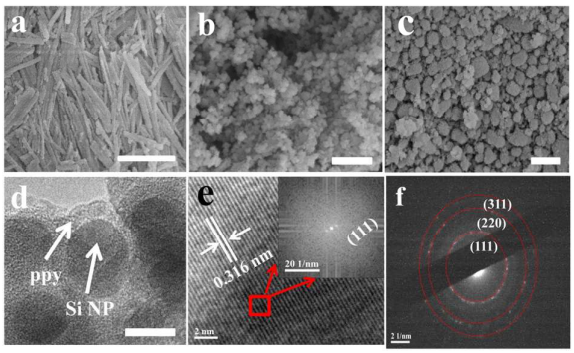

Fig. 3 SEM images of (a) the treated attapulgite clay, scale bar: 500 nm; (b) the obtained Si NPs, scale bar: 200 nm; (c) the ppy@Si nanocomposites, scale bar: 200 nm; (d) TEM image of the ppy@Si nanocomposites, scale bar: 10 nm; (e) HRTEM image (insert shows the FFT pattern) and (f) the SAED pattern of the Si NPs.

The PXRD pattern of the product after magnesiothermic reduction was shown in **Fig. 2c**. It could be seen the characteristic diffraction peaks of Si, besides the peaks of the byproduct MgO. After washing with dilute HCl and HF, pure Si NPs were obtained (**Fig. 2d**). The magnesium reductions of nanostructured silica have been used to produce silicon replicas by replacing the dense silica walls with 10-17 nm silicon crystallites.[27,28] In this work, it is postulated that the nanorods of attapulgite were cracked and reduced to Si nanoparticles under magnesiothermic conditions. Limited by the width of the attapulgite nanorods, the obtained Si NPs are small and uniform, with size around 10.5 nm (**Fig. 3b**, **Fig. 3d and Fig. S2**), which is in agreement with the particle size of 13.8 nm determined from the XRD data by using Debye-Scherrer formula. The high-resolution transition electron microscopy (HR-TEM) image of Si NPs showed that the lattice fringe of ~0.316 nm (**Fig. 3e**), and the Fast Fourier Transform (FFT) pattern of the selected area (red square). Both confirmed the formation of Si nanocrystals. Meanwhile, the selective area electron diffraction (SAED) pattern in **Fig. 3f** also confirmed that the obtained Si nanocrystals are of cubic phase.

The Energy Dispersive Spectroscopy (EDS) analysis of Si NPs (**Fig. 4a**) showed the atomic ratio of Si/O is about 4, indicating that the oxygen on the surface of Si nanoparticles had been reduced to some extent after washed with dilute HF solution. Raman spectrum of Si NPs was shown in **Fig. 4b.** The peak located at 520 cm^{-1} is attributed to the crystalline silicon, in consistent with the TEM and EDS analyses. Notably, the obtained Si NPs showed a Brunauer–Emmett–Teller (BET) specific surface area of 132 $m^2\ g^{-1}$, larger than that of attapulgite nanorods (94 $m^2\ g^{-1}$), which is ascribed to the smaller size of Si NPs induced by cracking of the nanorods (**Fig. 5a** and **Fig. 5b**).

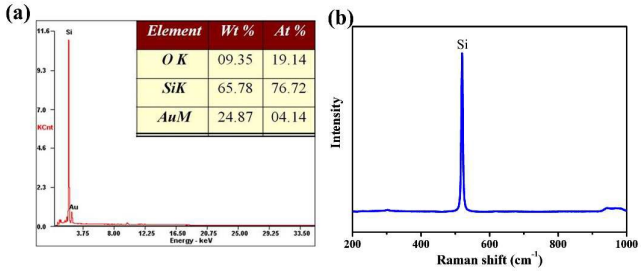

Fig. 4 (a) EDS spectra of Si NPs and (b) Raman spectra of Si NPs.

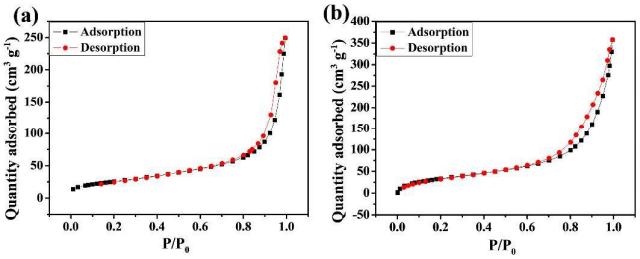

Fig. 5 N_2 adsorption isotherms of (a) SiO_2 nanorods derived from attapuligite and (b) Si NPs after magnesiothermic reduction.

To test the performance of Si NPs as LIB anode materials, Si NPs were coated with conductive polypyrrole to form ppy@Si nanocomposites according to the literature procedure.[29] **Fig. 2e** displayed the PXRD pattern of the ppy@Si nanocomposite. The

broad diffraction peak around 22° was ascribed to the formation of amorphous polypyrrole. The SEM and TEM images in **Fig. 3c** and **3d**, respectively, showed that the surfaces of the Si NPs were covered by amorphous ppy layers with a thickness of 5-10 nm. The sizes of the formed ppy@Si composites were apparently larger than those of bare Si NPs. The coated ppy were estimated to be ~30 wt% by thermogravimetric (TG) analyses (**Fig. S3**). **Fig. 6** shows the FT-IR spectra of ppy and ppy@Si nanocomposites, respectively. The peaks centered at 1545, 1450, 1293, 1167, 1037, 899, 799, 668 and 615 cm^{-1} in both spectra were ascribed to the characteristic vibrations of ppy.[30,31] The new peak around 470 cm^{-1} in ppy@Si nanocomposites was due to the Si-O vibration on the surface of Si NPs.

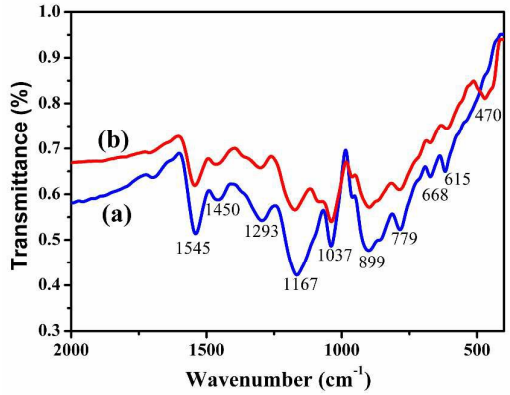

Fig. 6 FT-IR spectra of (a) ppy and (b) ppy@Si nanocomposites.

The ppy@Si nanocomposite anodes were assembled in 2025 Coin cells using lithium metal foil as the counter electrode. Cyclic voltammetry (CV) measurements for the ppy@Si nanocomposite anodes were carried out at 0.2 mV s^{-1} in the potential window of 0-3 V, which clearly showed the typical Si lithiation/delithiation processes (**Fig. 7a**). In the cathodic scan, there was a sharp cathodic peak below 0.1 V in the first and subsequent scans, which corresponds to the transformation of silicon from a crystalline phase to an amorphous one.[32] In addition, a broad irreversible cathodic peak that occurred at around ca. 0.65 V in the first scan but disappeared after subsequent cycles was ascribed to the formation of the solid electrolyte interface (SEI) membrane.[33] In the anodic scan, on the other hand, two peaks were observed around 0.34 V and 0.51 V, respectively, in the first charge process and retained nearly the same positions in the following scans. These two peaks can be attributed to the de-lithium of the Li-Si alloys.[34]

Fig. 7b displayed representative discharge-charge voltage profiles of the ppy@Si nanocomposite anodes for the first two cycles at a current density of 0.1 A g^{-1} and for the 100th cycles at a current density of 0.6 A g^{-1} in the potential window of 0.01-1.5 V, respectively. The specific discharge and charge capacities for the first cycle were 1486 and 808 mAh g^{-1}, respectively, indicating a coulombic efficiency of 54.4 %. The loss of irreversible capacity is mainly due to the formation of the SEI membrane, which results in the low coulombic efficiency.[35] The charging-discharging curves for the ppy@Si nanocomposite anodes presented two voltage plateaus at ~ 0.6 V and ~ 0.1 V during the first lithiation process, which were generally linked to the SEI formation and the lithiation process, respectively.[33] The results were consistent with those of the CV curves. Importantly, no obvious capacity decay was observed in the subsequent cycles, and the coulombic efficiency was maintained nearly constant at around 100%. A large voltage hysteresis between the charge and discharge plateau was seen in the first cycle, which was a common phenomenon because of polarization. Nonetheless, the voltage hysteresis was rather small in the subsequent cycles, implying good reaction kinetics for the ppy@Si nanocomposite anodes.[36]

The rate performance of the ppy@Si nanocomposites at different current densities varied from 0.3 to 3 A g^{-1} was shown in **Fig. 7c**. Before testing the rate performance and long-term cycling stability, the electrodes were pre-cycled at a low current density of 0.1 A g^{-1} for 10 cycles. Because the specific capacity of the ppy@Si nanocomposite gradually increased in the first few cycles at low current densities (as shown in **Fig. S4**), which was attributed to the gradual activation of the Si host.[25] The specific discharge capacities of the ppy@Si nanocomposite were 1635, 1498, 1294, 1158, 749 and 409 mAh g^{-1} at current densities of 0.3, 0.6, 0.8, 1.0, 1.5 and 3.0 A g^{-1}, respectively. The specific discharge capacity decreased gradually with increasing the current density. Remarkably, the cycle capacity was retained at each current density, even at a high current density of 3 A g^{-1}. Furthermore, the capacity could recover to the initial value after a deep charge-discharge measurement at high current densities, indicating a good reversibility of the ppy@Si nanocomposite anodes.

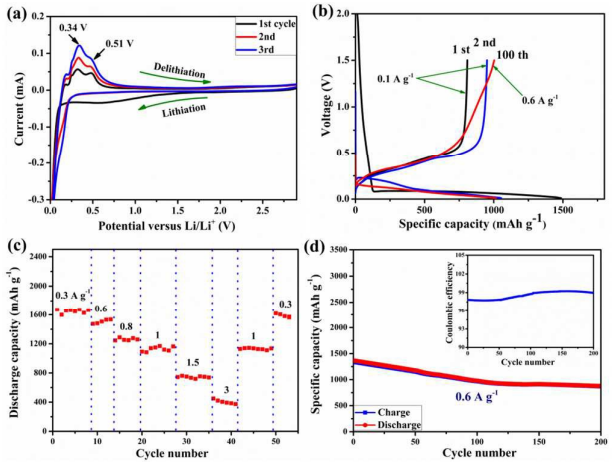

Fig. 7 (a) CV curves of the ppy@Si nanocomposites; (b) Voltage profiles of the ppy@Si nanocomposites; (c) Rate performance of the ppy@Si electrode cycled at various current densities, and (d) Cycling performance at current densities of 0.6 A g^{-1} (Insert shows the corresponding coulombic efficiencies).

The long-term cycling stability of the ppy@Si nanocomposite anodes was examined at a current density of 0.1 A g^{-1} for initial 10 cycles (**Fig. S4**) and 0.6 A g^{-1} for 200 cycles (**Fig. 7d**). After charge-discharge cycling for 200 cycles at the current density of 0.6 A g^{-1}, the specific capacity value

decreased from ~1294 to ~954 mAh g^{-1}, which corresponded to ~74% capacity retention. It is noted that the capacity degradation during the first 100 cycles was slightly severe when compared to the rest cycles, which is likely due to the pulverization of uncoated Si NPs. The good retention was mainly ascribed to the small Si sizes and the ppy coating, which reduce the diffusion-induced stress and buffer the volume change during the lithiation and delithiation processes.[29]

In order to investigate the cycling performance of ppy@Si nanocomposite anodes, the ppy@Si nanocomposite was removed from the cell after charging-discharging for 200 cycles. The morphology of ppy@Si nanocomposite was characterized with SEM and TEM after washing with acetonitrile. As shown in **Fig. 8**, despite the volume expansion was unavoidable, most of the particles kept the pristine morphology, and the ppy coating was still retained. Thus, the prepared ppy@Si nanocomposite showed good cycling stability as LIB anodes.

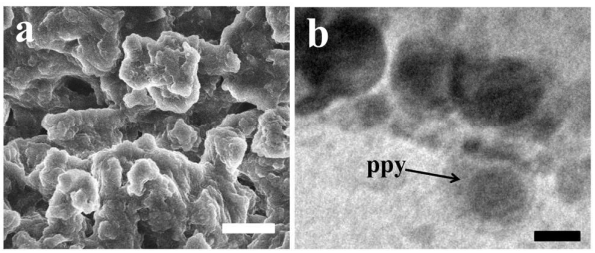

Fig. 8 (a) SEM image (scale bar: 200 nm) and (b) TEM image (scale bar: 10 nm) of ppy@Si nanocomposite anodes after charging-discharging for 200 cycles.

Conclusions

In summary, based on the magnesiothermic reaction, we report a new method for the synthesis of Si nanoparticles with uniform size around 10 nm by utilizing natural attapulgite clay as low-cost SiO_2 precursors. The produced Si NPs show excellent electrochemical properties when served as anode materials for the Li-ion battery. After charging-discharging for 200 cycles at a current density of 0.6 A g^{-1}, the capacity retention and the specific capacity values of the ppy@Si anode are ~74% and ~954 mAh g^{-1}, respectively. Because of the abundance of the attapulgite, the obtained silicon nanoparticles can be exploited as a practical anode material for high-performance Li-ion battery.

Acknowledgements

We are grateful for financial support from the National Natural Science Foundation of China (21471075).

Notes and references

[1] H. P. Zhang, X. Wu, T. Yang, S. S. Liang, and X. J. Yang, *Chem. Commun.,* 2013, **49**, 9977.
[2] L. Li, A. O. Raji, and J. M. Tour, *Adv. Mater.*, 2013, **25**, 6298.
[3] G. Y. Zheng, S.-W. Lee, Z. Liang, H.-W. Lee, K. Yan, H. B. Yao, H. T. Wang, W. Y. Li, S. Chu, and Y. Cui, *Nat. Nanotechnol.*, 2014, **9**, 618.
[4] S. Girl, S. Behera, and P. Jena, *Angew. Chem. Int. Ed.*, 2014, **53**, 13916.
[5] M. K. Y. Chan, C. Wolverton, and J. P. Greeley, *J. Am. Chem. Soc.*, 2012, **134**,14362.
[6] W. Sun, R. Z. Hu, H. Liu, M. Q. Zeng, L. C. Yang, and H. H. Wang, *J. Power Sources*, 2014, **268**, 610.
[7] X. L. Li, M. Gu, S. Y. Hu, R. Kennard, P. F. Yan, X. L. Chen, C. M. Wang, M. J. Sailor, J. G. Zhang, and J. Liu, *Nat. Commun.*, 2014, **5**, 4105.
[8] M. T. Mcdowell, I. Ryu, S. W. Lee, C. M. Wang, W. D. Nix, and Y. Cui, *Adv. Mater.*, 2012, **24**, 6034.
[9] M. Ebner, F. Marone, M. Stampanoni, and V. Wood, *Science*, 2013, **342**, 716.
[10] Y. He, D. M. Piper, M. Gu, J. J. Travis, S. M. George, S. H. Lee, A. Genc, L. Pullan, J. Liu, S. X. Mao, J. G. Zhang, C. M. Ban, and C. M. Wang, *ACS nano,* 2014, **8**, 11816.
[11] J. I. Lee, N. S. Chio, and S. Park, *Energy Environ. Sci*., 2012, **5**, 7878.
[12] B. Wang, X. L. Li, T. F. Qiu, B. Luo, J. Ning, J. Li, X. F. Zhang, M. H. Liang, and L. J. Zhi, *Nano Lett.*, 2013, **13**, 5578.
[13] C. Wang, H. Wu, Z. Chen, M. T. McDowell, and Y. Cui, Z. N. Bao, *Nat. Chem.*, 2014, **5**, 1042.
[14] M. Su, Y. Li, B. Maynor, A. Buldum, J. P. Lu, and J. Liu, *J. Phys. Chem.* B, 2000, **28**, 6505.
[15] D. P. Wei, and Q. Chen, *J. Phys. Chem. C*, 2008, **112** 15129.
[16] J. H. Warner, A. Hoshino, K. Yamamoto and R. D. Tilley, *Angew. Chem. Int. Ed.*, 2005, **44**, 4550.
[17] R. D. Tilley and K. Yamamoto, *Adv. Mater.*, 2006, **18** 2053.
[18] X. Y. Cheng, S. B. Lowe and P. J. Reece, J. Gooding, *Chem. Soc. Rev.*, 2014, **43**, 2680.
[19] Y. Yu, L. Gu, C. B. Zhu, S. Tsukimoto, P. A. V. Aken and J. Maier, *Adv. Mater.*, 2010, **22**, 2247.
[20] X. J. Feng, J. Yang, Y. T. Bie, J. L. Wang, Y. Nuli and W. Lu, *Nanoscale*, 2014, **6**, 12532.
[21] Z. Favors, W. Wang, H. H. Bay, Z. Mutlu, K. Ahmed, C. Liu, M. Ozkan and C. S. Ozkan, *Sci. Rep.*, 2014, **4**, 5623.
[22] W. S. Kim, Y. Hwa, J. H. Shin, M. Yang, H. J. Sohn and S. H. Hong, *Nanoscale*, 2014, **6**, 4297.
[23] D. S. Jung, M. H. Ryou, Y. J. Sung, S. B. Park and J. W. Choi, *Proc. Natl. Acad. Sci.*, 2013, **110**, 12229.
[24] A. Xing, S. Tian, H. Tang, D. Losic, Z. H. Bao, *RSC Advances*, 2013, **3**, 10145.
[25] J. Liu, P. Kopold, P.A. Aken, J. Maier and Y. Yu, *Angew. Chem. Int. Ed.*, 2015, **54**, 9632.
[26] W. F. Bradley, *Am. Mineral.*, 1940, **25**, 405.
[27] Z. Bao, M. R. Weatherspoon, S. Shian, Y. Cai, P. D. Graham, S. M. Allan, G. Ahmad, M. B. Dickerson, B. C. Church, Z. Kang, H. W. Abernathy, C. J. Summers, M. Liu and K. H. Sandhage, *Nature*, 2007, **446**, 172.
[28] M.-P. Liu, C.-H. Li, H.-B. Du and X.-Z. You, *Chem. Commun.*, 2012, **48**, 4950.
[29] F. H. Du, B. Li, W. Fu, Y. J. Xiong, K. X. Wang and J. S. Chen, *Adv. Mater*. 2014, **26**, 6145.
[30] J. B. Zhu, Y. L. Xu, J. Wang, J. P. Wang, Y. Bai and X. F. Du, *Phys. Chem. Chem. Phys.*, 2015, **17**, 19885.
[31] K. Z. Setshedi, M. Bhaumik, S. Songwane, M. S. Onyango and A. Maity, *Chem. Eng. J*, 2013, **222**, 186.
[32] Y. H. Xu, G. P. Yin, Y. L. Ma, P. J. Zuo and X. Q. Cheng, *J. Mater. Chem.*, 2010, **20**, 3216.
[33] Y. C. Yen, S. C. Chao, H. C. Wu and N. L. Wu, *J. Electrochem. Soc.*, 2009, **156**, A95.

[34] J. Y. Ji, H. X. Ji, L. L. Zhang, X. Zhao, X. Bai, X. B. Fan, F. B. Zhang and R. S. Ruoff, *Adv. Mater.*, 2013, **25**, 4673.
[35] B. M. Bang, J. I. Lee, H. J. Kim, J. Cho and S. Park, *Adv. Energy Mater.*, 2012, **2**, 878.
[36] H. Zhong, H. Zhan and Y. H. Zhou, *J. Power Sources*, 2014, **262**, 10.